AMERICAN SOCIETY FOR MICROBIOLOGY | mBio®

Check for updates

Identification of Zinc-Dependent Mechanisms Used by Group B *Streptococcus* To Overcome Calprotectin-Mediated Stress

Lindsey R. Burcham,[a] Yoann Le Breton,[b*] Jana N. Radin,[c] Brady L. Spencer,[a] Liwen Deng,[a] Aurélia Hiron,[e] Monica R. Ransom,[a] Jéssica da C. Mendonça,[a] Ashton T. Belew,[b,f] Najib M. El-Sayed,[b,f] Kevin S. McIver,[b] Thomas E. Kehl-Fie,[c,d] Kelly S. Doran[a]

[a]Department of Immunology and Microbiology, University of Colorado School of Medicine, Aurora, Colorado, USA
[b]Cell Biology and Molecular Genetics, University of Maryland, College Park, Maryland, USA
[c]Department of Microbiology, University of Illinois at Urbana—Champaign, Urbana, Illinois, USA
[d]Carl R. Woese Institute for Genomic Biology, University of Illinois at Urbana—Champaign, Urbana, Illinois, USA
[e]Université de Tours, INRAE, ISP, Tours, France
[f]Center for Bioinformatics and Computational Biology, University of Maryland, College Park, Maryland, USA

Yoann Le Breton, Jana N. Radin, Kevin S. McIver, and Thomas E. Kehl-Fie contributed equally to this article.

ABSTRACT Nutritional immunity is an elegant host mechanism used to starve invading pathogens of necessary nutrient metals. Calprotectin, a metal-binding protein, is produced abundantly by neutrophils and is found in high concentrations within inflammatory sites during infection. Group B *Streptococcus* (GBS) colonizes the gastrointestinal and female reproductive tracts and is commonly associated with severe invasive infections in newborns such as pneumonia, sepsis, and meningitis. Although GBS infections induce robust neutrophil recruitment and inflammation, the dynamics of GBS and calprotectin interactions remain unknown. Here, we demonstrate that disease and colonizing isolate strains exhibit susceptibility to metal starvation by calprotectin. We constructed a *mariner* transposon (*Krmit*) mutant library in GBS and identified 258 genes that contribute to surviving calprotectin stress. Nearly 20% of all underrepresented mutants following treatment with calprotectin are predicted metal transporters, including known zinc systems. As calprotectin binds zinc with picomolar affinity, we investigated the contribution of GBS zinc uptake to overcoming calprotectin-imposed starvation. Quantitative reverse transcriptase PCR (qRT-PCR) revealed a significant upregulation of genes encoding zinc-binding proteins, *adcA*, *adcAII*, and *lmb*, following calprotectin exposure, while growth in calprotectin revealed a significant defect for a global zinc acquisition mutant (Δ*adcA*Δ*adcAII*Δ*lmb*) compared to growth of the GBS wild-type (WT) strain. Furthermore, mice challenged with the Δ*adcA*Δ*adcAII*Δ*lmb* mutant exhibited decreased mortality and significantly reduced bacterial burden in the brain compared to mice infected with WT GBS; this difference was abrogated in calprotectin knockout mice. Collectively, these data suggest that GBS zinc transport machinery is important for combatting zinc chelation by calprotectin and establishing invasive disease.

IMPORTANCE Group B *Streptococcus* (GBS) asymptomatically colonizes the female reproductive tract but is a common causative agent of meningitis. GBS meningitis is characterized by extensive infiltration of neutrophils carrying high concentrations of calprotectin, a metal chelator. To persist within inflammatory sites and cause invasive disease, GBS must circumvent host starvation attempts. Here, we identified global requirements for GBS survival during calprotectin challenge, including known and putative systems involved in metal ion transport. We characterized the role of zinc import in tolerating calprotectin stress *in vitro* and in a mouse model of infection. We observed that a global zinc uptake mutant was less virulent than the pa-

rental GBS strain and found calprotectin knockout mice to be equally susceptible to infection by wild-type (WT) and mutant strains. These findings suggest that calprotectin production at the site of infection results in a zinc-limited environment and reveals the importance of GBS metal homeostasis to invasive disease.

KEYWORDS GBS, calprotectin, meningitis, nutritional immunity, zinc

Bacteria, like eukaryotes, have a strict requirement for transition metals that often function as enzyme cofactors or provide protein structural support (1). Though essential for survival, metal ions can also be toxic, and to successfully survive within a host, pathogens must coordinate ion uptake and efflux to maintain intracellular metal homeostasis (2–4). To antagonize the nutritional requirements of invading pathogens, the vertebrate host immune system has evolved elaborate mechanisms for restricting access to metal ions, a process termed nutritional immunity (5, 6). The hosts' efforts to limit access to metal ions can dampen pathogen metalloenzyme function, restricting growth and the ability to cause disease (7–9). Widely recognized host iron-binding proteins include transferrin, lactoferrin, and lipocalin-2 that sequester iron(III) or iron-bound siderophores (10–12) from pathogens. Calprotectin, another metal-binding host protein, is unique in that it can interact with multiple metal ions (2). Calprotectin is a tetraheterodimer of two members of the S100 protein family, S100A8/S100A9, or calgranulin A/B and MRP-8/14 (6, 13) and makes up approximately 50% of the neutrophilic cytoplasmic protein content (13). S100A8 and S100A9 form a heterodimer that, upon calcium-dependent conformational change, create two metal-binding sites that bind zinc with picomolar/femtomolar affinity (14–16) and manganese at nanomolar affinities (7, 16, 17). More recent studies have shown that calprotectin can additionally chelate iron(II) (18–20), copper (20, 21), and nickel *in vitro* (22), but the implications of the binding of these metals during infection are not understood. Calprotectin is abundant during inflammation or at sites of infection, where a stool concentration of >250 μg/g indicates active intestinal inflammation in patients with Crohn's disease (23, 24) and concentrations can exceed 1 mg/ml in tissue abscesses; therefore, invading pathogens must be able to cope with these pressures to cause disease (17, 25).

Streptococcus agalactiae, or group B *Streptococcus* (GBS), is a pathobiont that colonizes the vaginal tract but can be a severe threat to the fetus and newborn. The onset of GBS invasive disease in the neonate can occur as a result of aspiration during passage through a colonized birth canal (26), bacterial transmigration through the bloodstream (27), and penetration of the blood-brain barrier (BBB) (28). To combat the risk of infection in newborns, many countries have implemented the use of prophylactic antibiotics administered to colonized pregnant mothers at the time of delivery (29); however, despite these widespread efforts, GBS remains a leading cause of neonatal pneumonia, sepsis, and meningitis (30). Bacterial meningitis is a severe and potentially lethal pathology of the central nervous system that develops when pathogens overcome host defenses and successfully penetrate the BBB. Meningitis is characterized by an overwhelming cytokine response and immune cell influx to the site of infection (31). Meningitis is a particularly complex disease and results in a neonatal mortality rate as high as 40% (31, 32). Furthermore, the associated inflammation results in neuronal damage and brain injury, with nearly 20% to 50% of surviving patients suffering permanent neurological sequelae, including hearing and vision impairment, cognitive deficiencies, and seizures (33, 34).

During acute bacterial meningitis, neutrophils predominate in the cerebral spinal fluid, which is often used as a diagnostic marker. Following interaction with hu man cerebral microvascular endothelial cells (hCMEC) *in vitro*, GBS induces a characteristic neutrophilic inflammatory response, including expression of chemoattractants interleukin-8 (IL-8), C-X-C motif chemokine ligand 1 (CXCL-1), and CXCL-2 (35–37). Similar results are observed in animal models of experimental GBS meningitis, as brain tissue of GBS-infected mice shows increased neutrophil and monocyte infiltration compared to that of naive controls (37), indicating a close interaction between GBS and

granulocytic cells during active infection. Additional studies have shown that, in response to GBS, neutrophils elaborate extracellular traps decorated with lactoferrin (38) and that S100A9, a calprotectin subunit, is present in the blood and amniotic fluid during intrauterine GBS infection (39). These observations suggest that GBS experiences metal limitation during infection, but the mechanisms used by GBS to overcome nutritional immunity remain unknown.

Bacteria utilize a number of strategies to obtain zinc during infection, including direct uptake of the metal, the use of metallophores, and piracy from zinc-bound host proteins. While there is a myriad of strategies employed to obtain zinc, the AdcABC/ZnuABC family of ATP-binding cassette transporters are present in most bacteria. Streptococcal pathogens *S. pneumoniae* and *S. pyogenes* harbor two zinc-binding proteins, AdcA and AdcAII/Lmb, whereas GBS is particularly distinct as it possesses three zinc-binding proteins, AdcA, AdcAII, and Lmb (40, 41). AdcA and AdcAII/Lmb have been shown to utilize distinct mechanisms to bind zinc ions and shuttle them through the AdcBC transporter and are important for growth in zinc-restricted environments and infection (42–45).

Here, we investigated GBS fitness during calprotectin stress using a newly constructed saturated transposon mutant library and targeted amplicon sequencing. We characterized the global requirements for GBS survival during nutritional immunity, identifying 258 mutants, 123 underrepresented and 135 overrepresented, that impact calprotectin sensitivity. We show here that characterized and putative metal transporters are important for calprotectin survival *in vitro* and that the zinc uptake machinery contributes to survival during calprotectin-induced starvation and invasive disease progression. These results provide insight into zinc-dependent mechanisms that GBS employs to evade the host immune response and nutritional immunity to successfully cause disease and establish a groundwork to study the comprehensive effects of chelation on multimetal transport in GBS.

RESULTS

GBS growth inhibited in the presence of calprotectin. Previous studies have shown calprotectin inhibits bacterial growth by limiting nutrient metal ions (7–9). To characterize the response of GBS to metal chelation by calprotectin, we assessed growth of GBS strains in the presence of purified calprotectin. Disease clinical isolates A909 (serotype Ia) (46), CJB111 (serotype V) (47), and COH1 (serotype III) (48) were incubated with increasing concentrations of purified calprotectin ranging from 0 to 480 μg/ml, and growth was assessed by optical density and plating for viable bacteria. Although various levels of chelation sensitivity were detected, growth of all GBS strains (as measured by optical density at 600 nm [OD_{600}]) was significantly inhibited at high, but still physiologically relevant, calprotectin doses (Fig. 1A to C). Similar patterns of growth inhibition were observed when growth was assessed by enumerating CFU following an 8-h incubation with calprotectin. Exposure to calprotectin at concentrations higher than 120 μg/ml significantly inhibited growth of all GBS strains (Fig. 1D to F), while supplementation of zinc sulfate during calprotectin stress restored growth in all three strains (see Fig. S1A to C in the supplemental material). Additionally, we determined how a panel of 27 vaginal isolates collected from the vaginal tracts of pregnant women (49) survived in the presence of calprotectin. All strains were grown with or without 120 μg/ml calprotectin, and data are displayed as percent inhibition in treated versus untreated controls for isolates belonging to five different capsular serotypes. We observed a mean percent inhibition across the isolates that ranged from 30% to 55%. When mean inhibition of each serotype was compared against the others, we observed that vaginal isolates belonging to serotype V exhibited the most variability between strains and were significantly more resistant to calprotectin-mediated chelation than serotype Ia isolates (Fig. 1G). Representative invasive isolates A909, CJB111, and COH1 were included in the isolate panel in their capsular serotype grouping and are denoted by the open shapes in Fig. 1G. These data suggest that while there is
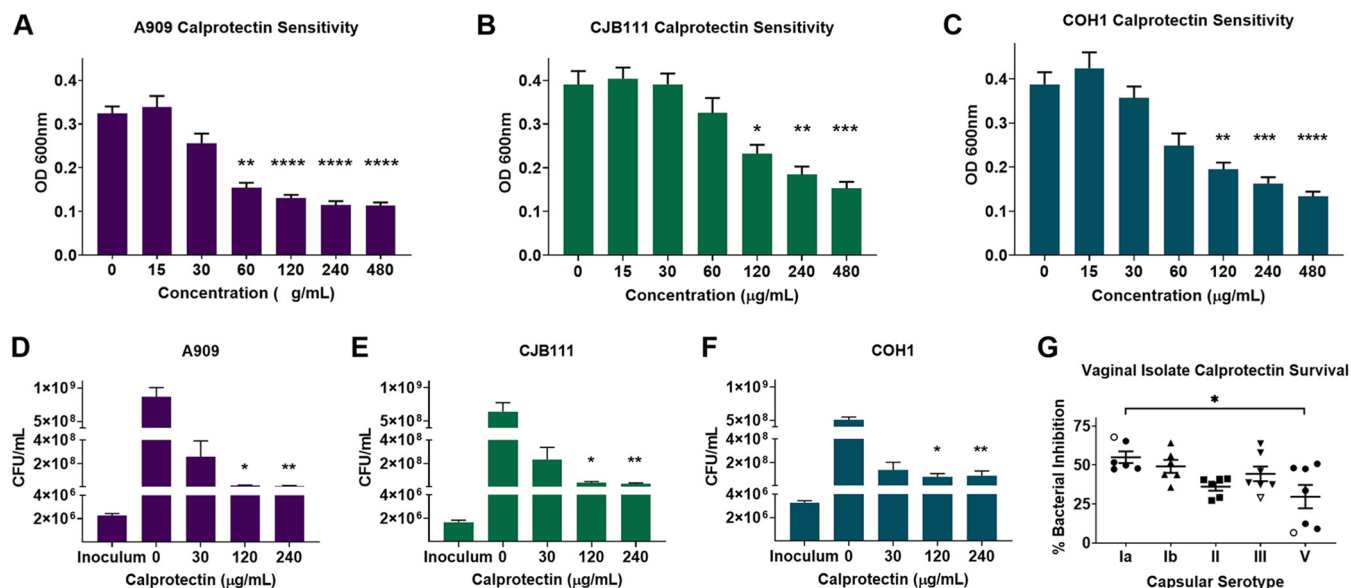
FIG 1 Calprotectin inhibits GBS growth *in vitro*. Growth of GBS invasive isolates A909 (A), CJB111 (B), and COH1 (C) was assessed by measuring optical density (OD$_{600}$) following an 8-h incubation with recombinant calprotectin (0 to 480 μg/ml) or by quantitating CFU (D to F). (G) Sensitivity was assessed by OD$_{600}$ across a panel of vaginal isolates (closed shapes) and invasive isolates (open shapes) following an 8-h incubation with 120 μg/ml calprotectin. Data are displayed as percent growth inhibition compared to that of untreated isolate controls. All experiments were performed in technical triplicates ($n = 3$), and data were averaged from three independent experiments. Significance for panels A to F was determined by Kruskal-Wallis with Dunn's multiple-comparison tests comparing treated samples to untreated controls. Significance for panel G was determined by one-way ANOVA with Tukey's multiple-comparison test. *, $P < 0.05$; **, $P < 0.01$; ***, $P < 0.001$; ****, $P < 0.0001$.

variation in levels of sensitivity across strains and serotypes, GBS is broadly sensitive to the antimicrobial activity of calprotectin.

Essential genes for GBS growth in calprotectin. To successfully colonize the host or survive within highly inflammatory environments during infection, GBS must cope with nutritional immunity and, specifically, metal limitation imposed by calprotectin. To identify factors that are important for responding to calprotectin-mediated chelation, we constructed a GBS saturated *Krmit* transposon (Tn) mutant library in the CJB111 strain background as described previously for group A *Streptococcus* (50). Analysis of the library revealed 68,857 unique insertion sites across the GBS genome (Fig. 2). To identify essential genes for GBS growth, we outgrew the Tn mutant library in Todd Hewitt broth with yeast extract (THY), modified RPMI medium (mRPMI), and mRPMI plus subinhibitory (60 μg/ml) and inhibitory (480 μg/ml) concentrations of calprotectin. We recovered CFU from these growth conditions, extracted genomic DNA, and prepared sequencing libraries as described in Materials and Methods. Transposon insertions were sequenced as previously described (51) with minor changes, and sequenced reads were mapped back to the GBS genome. Bayesian statistical analyses (52) identified, in the absence of calprotectin, 206 essential genes for growth in THY and 450 essential genes for growth in mRPMI (Fig. 3A and B), with 153 essential genes common to both media conditions (Fig. 3C; see also Table S1). The genes deemed essential for growth in THY and mRPMI were assigned clusters of orthologous groups of proteins (COGs) and were found to be involved primarily in translation, ribosomal structure, and biogenesis (23% in THY, 13% in mRPMI), replication, recombination, and repair (16% in THY, 13% in mRPMI), cell wall/membrane/envelope biogenesis (10% in THY, 10% in mRPMI), and carbohydrate transport and metabolism (10% in THY, 7% in mRPMI) (Fig. 3D and E).

Bayesian analyses were then used to determine the essential genes for growth in the presence of calprotectin. These analyses compared essential genes from the base medium (mRPMI) and subinhibitory and inhibitory concentrations of calprotectin. From these analyses, we identified 40 genes that were essential specifically for growth in mRPMI, 30 genes that were essential only for growth in a subinhibitory dose of calprotectin, and 55 genes that were essential only for growth in an inhibitory calpro-
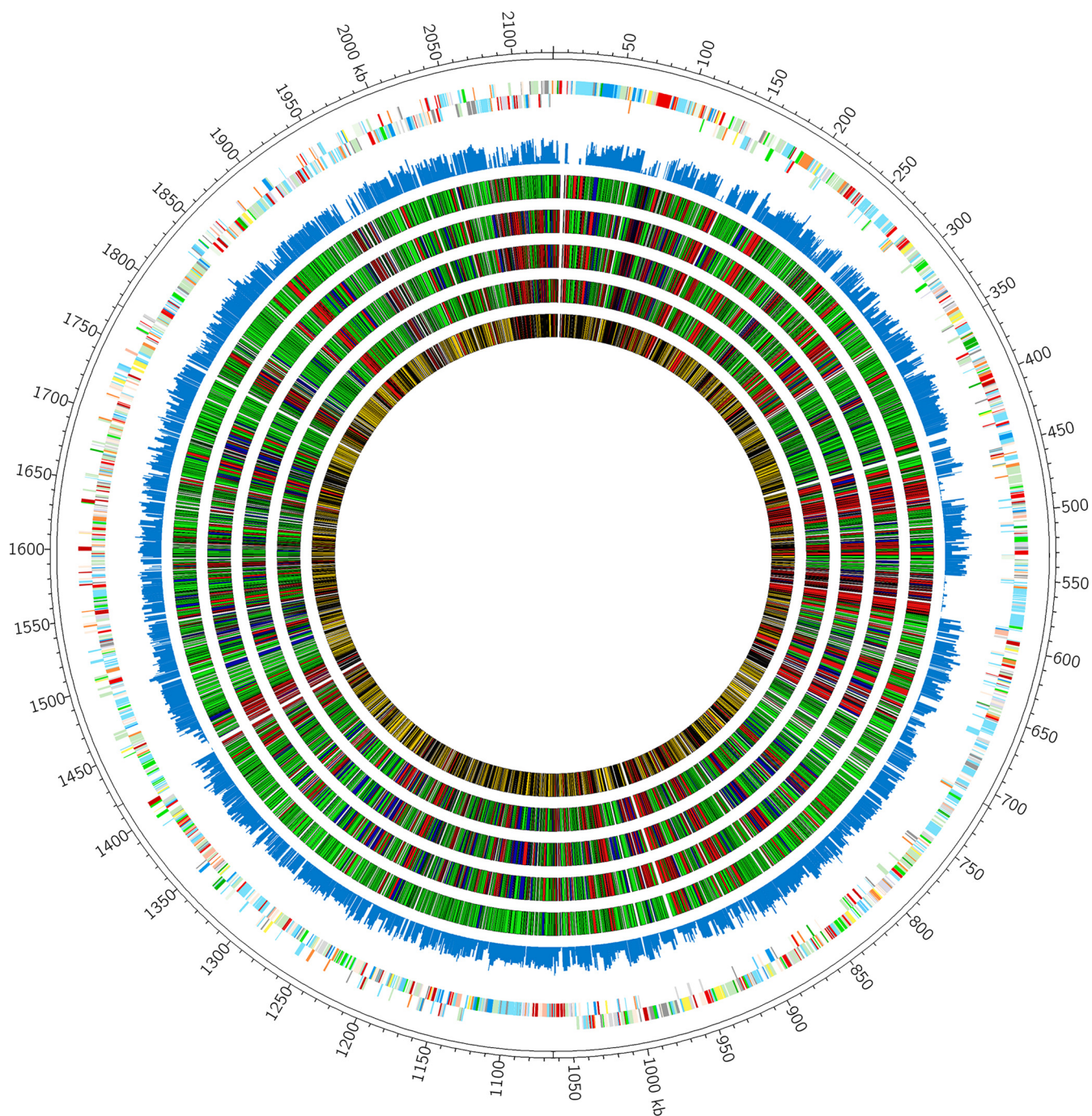
FIG 2 Construction of a saturated *Krmit* transposon mutant library in GBS. CIRCOS atlas representation of the A909 genome is shown with base pair (bp) ruler on the outer ring. The next two interior circles represent GBS open reading frames on the (+) and (−) strands, with colors depicting COG categories. The next circle (blue) indicates the frequency of *Krmit* transposon insertion site (TIS) observed in the initial mutant library grown in THY, with 68,857 unique insertion sites detected. The inner four circles present the results of Bayesian analysis of GBS gene essentiality under different growth conditions (THY, mRPMI, mRPMI plus subinhibitory calprotectin, and mRPMI plus inhibitory dose calprotectin, in order toward center; essential genes (red), nonessential genes (green), and excluded genes in either gray (too small for analysis) or black (inconclusive call). The center circle compiles the summary analysis of GBS genes under all four growth conditions, with essential genes under all conditions (red), nonessential genes under all conditions (yellow), and small/inconclusive genes (gray/black).

tectin dose. The remaining 306 essential genes were deemed important for growth across all environments (mRPMI, subinhibitory calprotectin, and inhibitory calprotectin) (Fig. 3F and G; Table S1).

Global impact of calprotectin on GBS fitness. To determine the global effect of calprotectin on GBS fitness, differential analyses were performed using DESeq2 com-
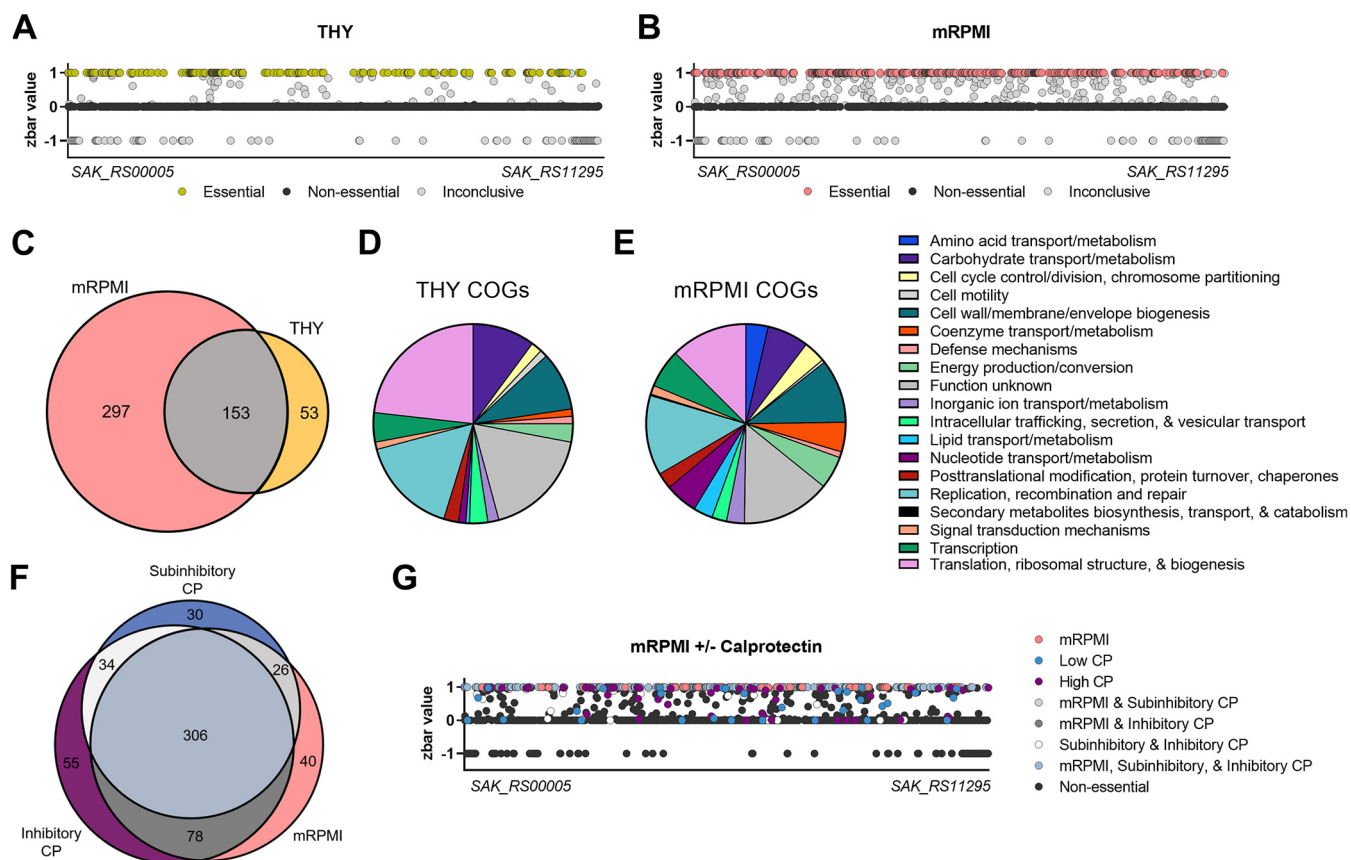
FIG 3 GBS essential genes for growth *in vitro*. Bayesian analysis of essential genes for growth in THY (A) or mRPMI (B). Essential genes are depicted as yellow (A) or pink (B), nonessential genes are shown in black, and inconclusive genes are shown in gray. The *x* axis is a linear representation of the A909 genome. EggNOG 5.0 was used to assign COGs to determine functions for essential genes for growth in THY (D) and mRPMI (E). Venn diagrams depict the essential genes for growth in mRPMI and THY (C) or mRPMI and subinhibitory (60 μg/ml) and inhibitory (480 μg/ml) calprotectin (F). (G) Linear map represents Bayesian analyses of essential genes for growth in mRPMI and subinhibitory and inhibitory calprotectin.

paring samples treated with subinhibitory (60 μg/ml) or inhibitory (480 μg/ml) calprotectin and untreated mRPMI controls. Genes found to be essential for growth in mRPMI (pink), subinhibitory calprotectin (blue), inhibitory calprotectin (purple), or across two treatments (gray) were excluded from fitness analyses (Fig. 4A and B). We characterized the global impact of calprotectin stress on GBS growth and identified a total of 258 mutants in the output pool whose growth was significantly impacted by calprotectin. We identified 135 mutations that conferred a fitness advantage for GBS during calprotectin stress, with 94 mutants in subinhibitory-dose and 98 mutants in inhibitory-dose calprotectin (Fig. 4A and B; Table S1), with 57 mutants common between the two calprotectin treatment groups. We also identified 123 mutants that resulted in a fitness defect during calprotectin stress; of those, 93 mutants were important in the subinhibitory dose of calprotectin and 76 mutants were important in the inhibitory levels of calprotectin (Fig. 4A and B; Table S1), with 46 mutants observed in both calprotectin-treated samples (Fig. 4C). Of the Tn mutants that were identified as underrepresented following treatment with calprotectin, COGs were identified for 76 of the mutations observed in subinhibitory treatment and 60 of the mutations observed in inhibitory calprotectin treatment. The most abundant COGs of known function were those involved in inorganic ion transport, amino acid and carbohydrate transport and metabolism, and defense (Fig. 4D and E). Approximately 15% of the mutants underrepresented in both concentrations were grouped into the inorganic ion COG and were previously characterized or putative systems involved in metal ion uptake or efflux (Table 1). These systems involved in maintaining metal homeostasis were many of the
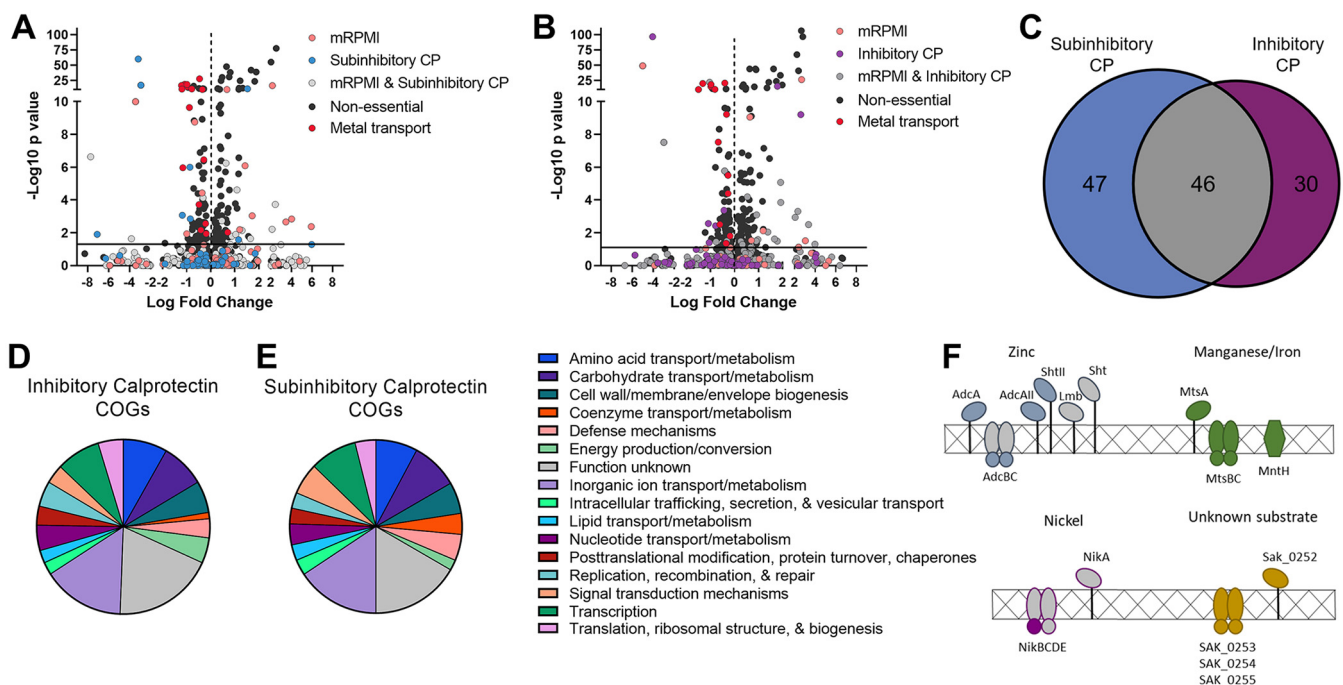
FIG 4 GBS genomic fitness screen in calprotectin. Volcano plots identify essential genes for growth in mRPMI and subinhibitory (60 μg/ml) calprotectin (A) and inhibitory (480 μg/ml) calprotectin (pink, blue/purple, and gray) (B) as well as nonessential genes (black) and genes involved in metal transport (red). (39). Essential genes (all but "nonessential" and "metal transport") were excluded from fitness analyses by DESeq2. (C) Venn diagram depicts the underrepresented mutants detected in low (60 μg/ml) and high calprotectin (480 μg/ml) and common genes important for growth under both conditions. COGs were assigned to genes that contribute to survival in subinhibitory dose (B) and inhibitory dose (C) of calprotectin using EggNOG 5.0. (F) Schematic of GBS metal importers that contribute to survival during calprotectin stress.

most significantly underrepresented mutants as denoted in the volcano plots (shown in red) for each calprotectin concentration (Fig. 4A and B).

To gain more insight into how the identified metal transport systems may contribute to homeostasis, all proteins of interest were clustered by ortholog against characterized metal transport machinery in the closely related *Streptococcus pneumoniae* TIGR4 genome. Of the three genes encoding zinc-binding proteins, we identified only *adcA* (SAK_0685) and *adcAII* (SAK_1898) as important for growth in calprotectin. The gene encoding their cognate ATPase, *adcC* (SAK_0218), and one of the genes encoding

TABLE 1 Genes encoding metal transporters implicated in survival in calprotectin

| Locus tag	Name	Description	*P* value control vs. calprotectin at:	
			Subinhibitory dose	Inhibitory dose
SAK_0218	*adcC*	Zinc ABC transporter, ATP-binding protein	0.01132	0.00004049
SAK_0252	SAK_0252	Peptide/opine/nickel uptake ABC transporter, substrate-binding protein	2.713E−15	1.019E−15
SAK_0253	SAK_0253	Peptide/opine/nickel uptake ABC transporter, permease protein	2.396E−19	4.972E−11
SAK_0254	SAK_0254	Peptide/opine/nickel uptake ABC transporter, permease protein	1.971E−17	1.16E−20
SAK_0255	SAK_0255	Peptide/opine/nickel uptake ABC transporter, ATP-binding protein	3.388E−19	7.2E−19
SAK_0514	*czcD*	Cation efflux transporter, cation diffusion facilitator (CDF) family	0.002825	0.01577
SAK_0515	*scZA*	Transcriptional regulator, TetR family	3.515E−07	0.00000315
SAK_0516	SAK_0516	Transcriptional regulator, AraC family	7.831E−11	6.017E−10
SAK_0685	*adcA*	Zinc ABC transporter, zinc-binding protein	2.612E−28	2.018E−21
SAK_0871	*mntH*	Mn^{2+}/Fe^{2+} transporter, NRAMP family	0.006823	0.04543
SAK_1539	*nikE*	Nickel ABC transporter, ATP-binding protein	0.04795	
SAK_1554	*mtsC*	Metal ABC transporter, permease protein	9.914E−12	
SAK_1555	*mtsB*	Metal ABC transporter, ATP-binding protein	2.325E−10	
SAK_1556	*mtsA*	Metal ABC transporter, metal-binding lipoprotein	1.381E−11	0.003134
SAK_1897	*shtII*	Streptococcal histidine triad family protein	0.0001926	2.972E−08
SAK_1898	*adcAII*	Laminin-binding surface protein		0.04445
SAK_2051	*cadD*	Cadmium resistance protein	0.000001093	6.657E−11
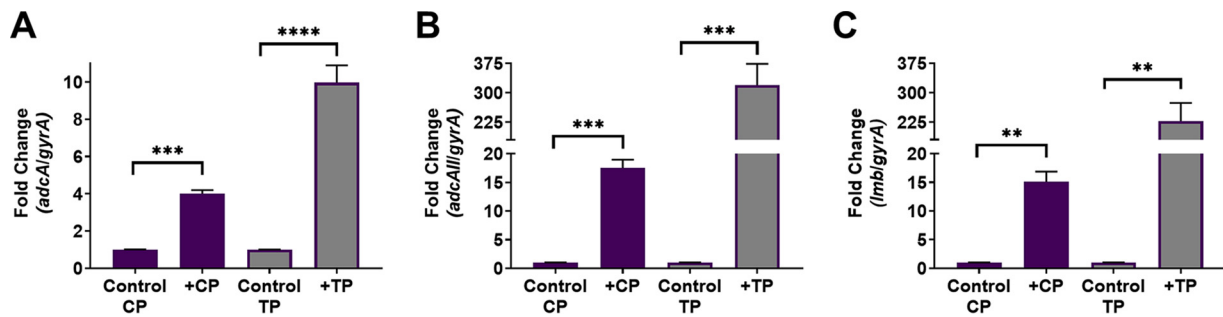
FIG 5 Zinc transport contributes to calprotectin resistance. Quantitative RT-PCR was used to assess expression of *adcA* (A), *adcAII* (B), and *lmb* (C) following exposure to 120 μg/ml calprotectin (CP) or 25 μM TPEN (TP). Fold change was calculated by $\Delta\Delta C_T$ analysis with *gyrA* serving as the internal control. Data are displayed as the average fold change from three independent experiments. Significance was determined by unpaired Student's *t* tests. **, $P < 0.01$; ***, $P < 0.001$; ****, $P < 0.0001$.

a streptococcal histidine triad protein, *shtII* (*SAK_1897*), were also underrepresented in our Tn sequencing analyses (Fig. 4F). Underrepresentation of mutants in *adcAII* was specific to treatment with inhibitory levels of calprotectin, while mutants in the remaining zinc transport genes detected were defective in calprotectin survival independent of concentration (Table 1).

In addition to the zinc machinery, significant underrepresentation was detected for Tn insertions in the genes encoding the manganese/iron ABC transporter, *mtsABC* (*SAK_1554-1556*), and the gene encoding the manganese/iron natural resistance-associated macrophage protein (NRAMP), *mntH* (*SAK_0871*) (53) (Fig. 4F). Ortholog clustering again confirmed the conservation of the GBS transporter MtsABC to the pneumococcal transporter PsaABC (53, 54); however, other pathogenic streptococci, including *S. pyogenes* and *S. pneumoniae*, are devoid of manganese- and iron-dependent NRAMP transporters (55–57). Additionally, mutants in genes that comprise two other putative metal ion uptake systems were identified as underrepresented (Fig. 4F). *nikD* (*SAK_1539*) is an ATP-binding protein encoded within the operon *nikABCDE* (*SAK_1538-1542*) that encodes a putative but uncharacterized nickel ABC transport system, and the second underrepresented and uncharacterized ABC transport system is encoded by *SAK_0252-0255*; however, the substrate transported by this system remains unknown (Fig. 4F). The substrate-binding proteins of both putative metal transport systems belong to the NikA/DppA/OppA superfamily.
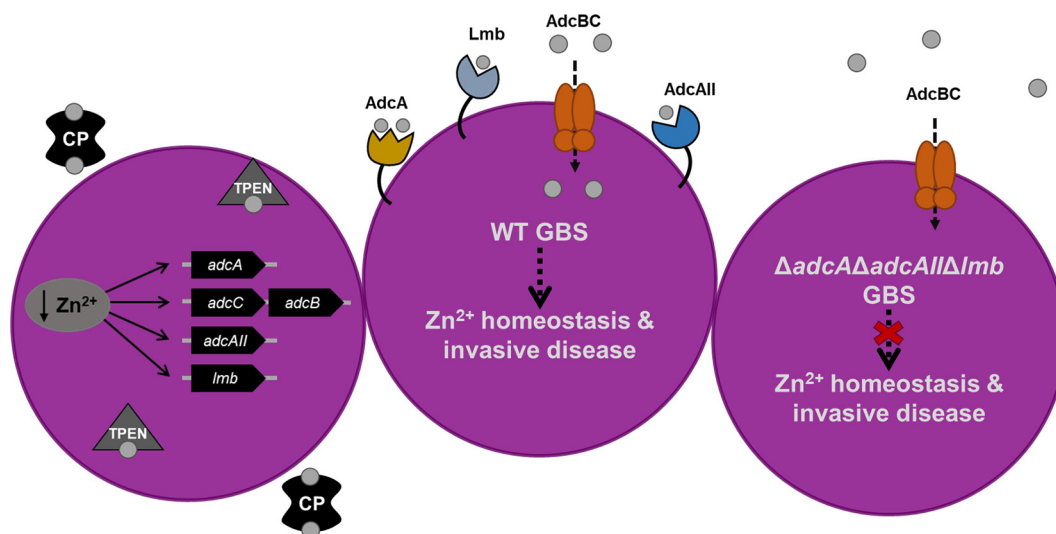
Calprotectin induces expression of zinc import machinery. Upon identifying mutants in genes encoding two zinc-binding proteins, *adcA* and *adcAII*, in our transposon sequencing analyses, we hypothesized that differential expression of genes involved in zinc acquisition might occur following exposure to calprotectin, a natural source of zinc limitation. Quantitative reverse transcriptase PCR (qRT-PCR) analysis of genes encoding the zinc-binding proteins *adcA*, *adcAII*, and *lmb* was performed following treatment with calprotectin or the cell membrane permeable chelator N,N,N',N'-tetrakis(2-pyridinylmethyl)-1,2-ethanediamine (TPEN). TPEN chelates zinc with an extremely high affinity (dissociation constant [K_d] = 10^{-15} M); however, it has been shown to bind other metal ions, including nickel (58), iron (59), and copper (60). Fold changes in gene expression were calculated by the comparative threshold cycle ($\Delta\Delta C_T$) with *gyrA* serving as an internal control and were compared to expression observed in untreated controls. Expression of *adcA* was induced 4-fold following exposure to calprotectin and 10-fold following TPEN treatment, while expression of *adcAII* and *lmb* was more robustly upregulated, with 18- and 15-fold inductions, respectively, in response to calprotectin treatment and 320- and 227-fold inductions, respectively, after treatment with TPEN (Fig. 5A to C). Expression of *SAK_0514*, ortholog to the cation diffusion facilitator encoded by *czcD* of *S. pneumoniae*, was also assessed by qRT-PCR to confirm that calprotectin and TPEN were inducing zinc-limited conditions. As expected, expression of *czcD* was downregulated following exposure to both (see Fig. S2A). To confirm what was previously described for GBS in zinc-limited chemically
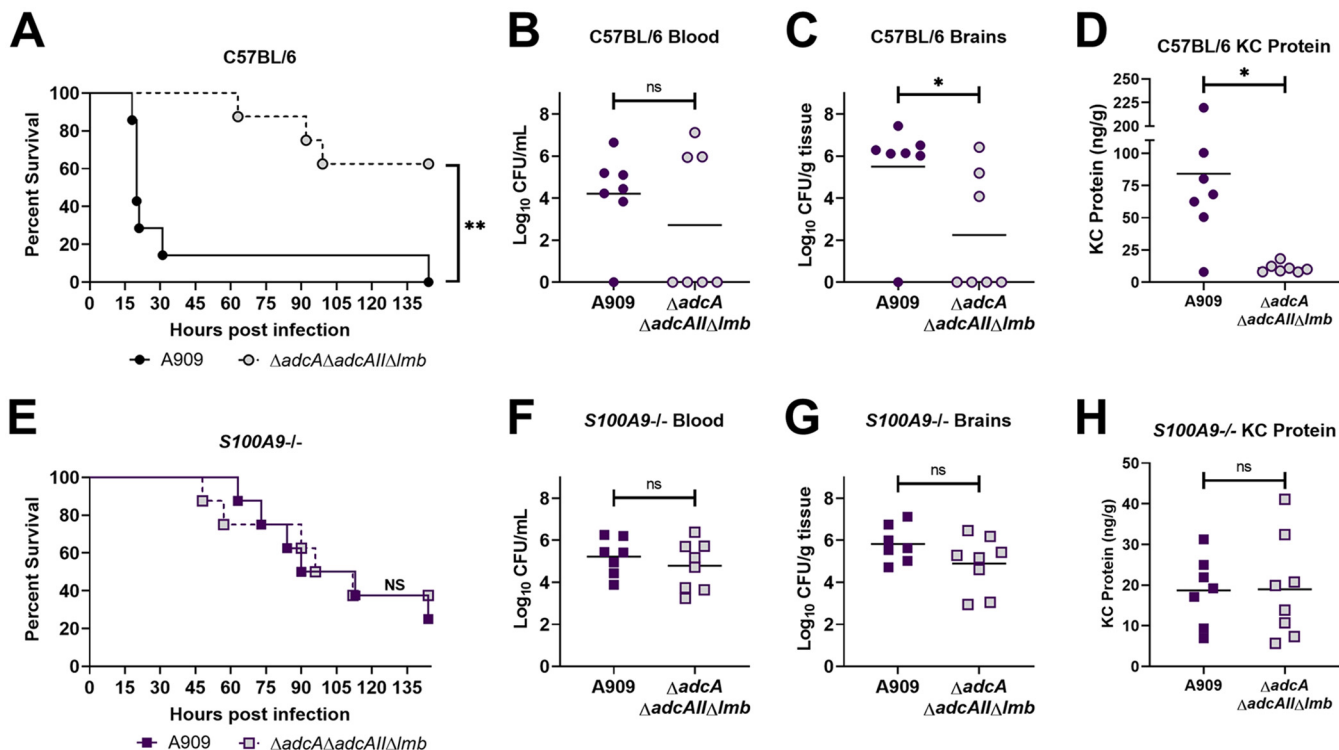
FIG 6 GBS zinc homeostasis contributes to calprotectin survival *in vivo*. Kaplan-Meier plot showing survival of C57BL/6 (A) or *S100A9*$^{-/-}$ (E) mice infected with 3×10^8 CFU of WT (solid line) or the Δ*adcA*Δ*adcAII*Δ*lmb* mutant (dotted line). Recovered CFU were quantified from brain tissue homogenates (B and F) or blood (C and G). (D and H) Cytokine abundance was quantified from brain tissue homogenates by ELISA. Statistical analyses include log rank (Mantel-Cox) tests for panels A and E and unpaired Student's *t* tests for panels B to D and F to H. *, $P < 0.05$; **, $P < 0.01$; ns, not significant.

defined medium (40, 41), we observed that mutants lacking individual zinc-binding proteins exhibited similar calprotectin sensitivity as the wild-type (WT) GBS strain, while growth of a triple Δ*adcA*Δ*adcAII*Δ*lmb* mutant was reduced (Fig. S2B). An increased sensitivity to calprotectin was also observed in a triple Δ*adcA*Δ*adcAII*Δ*lmb* mutant compared to that for the WT in both A909 and CJB111 strain backgrounds (Fig. S2C and D). These significant differences, though subtle are consistent with previous results that demonstrate functional redundancy exists between zinc-binding proteins and suggest that additional transport systems could be contributing to survival during calprotectin stress.

Zinc homeostasis contributes to GBS virulence and meningitis. Our results thus far suggest that GBS utilizes zinc uptake machinery to cope with calprotectin stress *in vitro*; thus, we hypothesized that zinc homeostasis would contribute to GBS virulence. Using a murine model of GBS systemic infection, we infected mice (C57BL/6) intravenously with the A909 WT or the isogenic Δ*adcA*Δ*adcAII*Δ*lmb* mutant strain. Infection with the WT GBS strain resulted in significantly higher mortality than with the mutant strain (Fig. 6A). By 36 h postinfection, 7/8 WT infected mice succumbed to infection. Conversely, only 3/8 mice challenged with the Δ*adcA*Δ*adcAII*Δ*lmb* strain succumbed to infection by the experimental endpoint of 144 h (Fig. 6A). At the time of death or the experimental endpoint, blood and brains were harvested to determine bacterial load. Despite similar levels of bacterial CFU recovered from blood (Fig. 6B), a significantly higher bacterial burden was observed in brain tissue (Fig. 6C) of WT GBS-infected animals than in animals infected with the Δ*adcA*Δ*adcAII*Δ*lmb* mutant strain. We further detected an increase in KC, a neutrophil chemokine, in brain homogenates of mice challenged with WT GBS compared to that in the Δ*adcA*Δ*adcAII*Δ*lmb* mutant strain (Fig. 6D), suggesting a more robust infection and increased inflammation in WT-infected mice. Similar results were also observed in the GBS CJB111 background (see Fig. S3A to D) and during infection in another mouse (CD-1) background (Fig. S3E to G).

FIG 7 Summary of the GBS zinc-dependent response to calprotectin. GBS senses metal limitation in the presence of calprotectin and induces expression of three zinc-binding proteins to acquire zinc and overcome starvation. GBS that is capable of regulating zinc homeostasis in a zinc-limited environment remains virulent, whereas GBS zinc transport mutant strains are deficient in their ability to cause invasive disease.

To determine the contribution of calprotectin specifically to GBS disease progression, we infected $S100A9^{-/-}$ mice with WT and $\Delta adcA\Delta adcAII\Delta lmb$ GBS. We observed that $S100A9^{-/-}$ mice were equally susceptible to WT and mutant GBS (Fig. 6E) and had similar bacterial loads in the brain and blood (Fig. 6F and G) and levels of neutrophilic chemokine KC in brain tissue (Fig. 6H). Interestingly, $S100A9^{-/-}$ mice were less susceptible to WT GBS infection than WT mice. Taken together, these data indicate that GBS zinc homeostasis is required for invasive disease, specifically, in the presence of host calprotectin.

DISCUSSION

GBS infections are known to result in increased immune cell influx and inflammation, specifically, neutrophilic infiltrate (35, 61). As these are characteristic signs of bacterial meningitis, GBS would encounter high concentrations of granulocyte-derived calprotectin (62) during infection. Calprotectin makes up more than 50% of the neutrophil cytosol and has been proven to be an effective molecule at starving incoming pathogens of nutrient metal ions (7, 63). However, despite this mechanism employed by the immune system to impede bacterial growth, GBS continues to cause life-threatening illnesses, suggesting that this bacterium possesses machinery to thwart host defenses and permit survival. Here, we have examined the global effect of calprotectin stress on GBS fitness using a newly developed *mariner* GBS transposon mutant library. We identified systems involved in zinc and manganese/iron homeostasis as well as putative metal-transport systems that were not previously described in GBS to be important for growth in the presence of calprotectin. Through mutagenesis and functional analyses, we determined that the Adc zinc acquisition system, comprising three zinc-binding proteins, promotes survival during calprotectin stress and contributes to systemic infection *in vivo*. Furthermore, the loss of calprotectin *in vivo* ablates the requirement of zinc homeostasis for GBS virulence. These data support the growing appreciation for the role of zinc uptake in bacterial pathogenesis and provide new insight into the mechanisms by which GBS resists nutritional immune challenge (Fig. 7).

In this study, we demonstrate, for the first time, the global impact of calprotectin-mediated metal chelation on GBS fitness using transposon library screening. We observed that growth of both GBS disease and colonizing clinical isolates was inhibited by physiologically relevant concentrations of recombinant calprotectin. Serotype V isolates were significantly more resistant to chelation than serotype Ia isolates *in vitro*,

but the basis for this requires further investigation. As our current understanding of GBS metal homeostasis is limited, we sought to characterize the global effects of calprotectin-mediated metal chelation on GBS fitness, utilizing a newly constructed *Krmit* transposon mutant library. This screen identified COG categories of GBS gene function during calprotectin stress, with the most abundant genes of known function involved in inorganic ion transport, amino acid and carbohydrate transport and metabolism, transcription, cell wall biogenesis, and defense mechanisms. Some of the most significant underrepresented factors identified were those involved in metal transport, including zinc/manganese/iron uptake and efflux. Our data also identified GBS essential genes for growth in rich media, including THY and mRPMI, and our results were consistent with a previous study using transposon sequencing of a different GBS strain, which identified essential genes in tRNA synthesis pathways, glycolysis, and nucleotide metabolism (64). We did, however, observe some differences. The transcriptional regulator *ccpA* was previously deemed part of the GBS essential genome (64), though in our analysis, *ccpA* was only essential in mRPMI. Similarly, the global nutritional regulator *codY*, which is essential for *Streptococcus pneumoniae* growth (65) and nonessential for GBS in rich medium (64), was found in our study to be nonessential for growth in THY but essential for GBS growth in mRPMI. Together, these data suggest that the essential genome of GBS is largely similar across strains, although this is dependent on the growth medium.

To survive in metal-limited environments, bacterial pathogens possess tightly regulated, high-affinity metal uptake systems, and many Gram-positive bacteria are known to use the ZnuABC/AdcABC zinc transport systems (66–68). In the case of pathogens such as *Staphylococcus aureus* and *Bacillus anthracis*, each possesses a single zinc-binding protein, AdcA and ZnuA, respectively (69, 70), and their associated ATP-binding cassette transporter permease and ATPase are AdcB/ZnuB and AdcC/ZnuC (40, 71). The zinc uptake machinery of streptococcal pathogens *S. pneumoniae* and *S. pyogenes* possess two zinc-binding lipoproteins, AdcA and AdcAII/Lmb. GBS is particularly unique in that in addition to AdcA and AdcAII, it harbors a third zinc-binding protein, annotated as Lmb (72), encoded on a mobile element that is cotranscribed with a second streptococcal histidine triad protein, ShtII. Lmb is thought to have been acquired by horizontal gene transfer and shares homology with Lsp of *Streptococcus pyogenes* (73), but the direct origin remains unknown. Originally annotated as laminin-binding proteins, Lmb and Lsp were thought to contribute to adherence, though this interaction has been debated and may be species or strain dependent (44, 74, 75). The GBS zinc uptake machinery is encoded by four distinct operons and is under the regulation of the zinc-dependent AdcR repressor (40). AdcR is involved in maintaining intracellular zinc homeostasis and has been shown to be important for growth under zinc-limited conditions (40, 41). Components of this system are also significantly upregulated during GBS murine vaginal colonization and following incubation with human blood (76, 77). In addition to the ABC transporters, bacteria have evolved other mechanisms to maintain zinc homeostasis, examples include the metallophore staphylopine produced by *Staphylococcus aureus* that binds zinc ions and is imported by the CntABCDF machinery (70) and the TdfH transporter of *Neisseria gonorrhoeae* that binds calprotectin directly to hijack and secure zinc ions (78). Although, similar systems have not been described in GBS.

Our transposon mutant screen during calprotectin treatment identified loss-of-function mutations in the zinc-binding protein AdcA as the most significantly underrepresented metal mutation. Mutants in the AdcC subunit of the zinc-dependent ABC transporter, zinc-binding proteins AdcA and AdcAII, and the streptococcal histidine triad protein ShtII were also underrepresented in our screen. Interestingly, mutations in Lmb and Sht did not result in fitness defects in our transposon library screen, suggesting that in a competitive growth environment, loss of either AdcA or AdcAII reduced GBS fitness in the presence of calprotectin. However, in monoculture, while loss of all three solute-binding proteins sensitized GBS to calprotectin, their individual losses did not. Expression of *adcAII* and *lmb* were both induced to greater extent than *adcA* by

both calprotectin and TPEN, and mutations in AdcAII were specifically observed in inhibitory calprotectin treatment. Collectively, these observations could indicate that the GBS zinc importers may uniquely contribute to resisting metal limitation or other aspects of infection, but further investigation is needed.

Additional systems of interest that were underrepresented in our calprotectin transposon library screen were *mtsABC* (*SAK_1554* to *1556*), *mntH* (*SAK_0871*), *sczA* (*SAK_0515*), *czcD* (*SAK_0514*), and *cadD* (*SAK_2051*). *mtsABC* encodes the manganese/iron-dependent ABC transporter, and *mtsA* is a component of the core GBS genome and could be a conserved system for survival during calprotectin-mediated stress within the host (53, 79). Additionally, *mntH* encodes the manganese/iron NRAMP and is known to be important for survival under acidic conditions similar to what GBS would encounter during inflammation or within the phagolysosome (57). Similar to what has been shown for zinc import, the *mtsABC* transporter was shown to be upregulated in human blood and during vaginal colonization (76, 77). In the context of metal ion efflux, we identified mutations in *sczA*, *czcD*, and *cadD*, which all resulted in fitness defects when grown in media containing calprotectin. SczA is a zinc-dependent transcriptional activator of the cation diffusion facilitator protein CzcD. This system has been shown to contribute to bacterial survival during zinc toxicity, neutrophil and macrophage killing, and GAS virulence (80–83). To date, SczA has been suggested to be an activator in GBS (80), but the functional roles of SczA and CzcD in metal efflux and GBS survival have not been described. Additionally, the *cadDX* operon in *Streptococcus salivarius* has been shown to have both cadmium- and zinc-inducible repression (84); thus, CadD may function similarly in GBS, but this warrants further investigation. Recently, a new highly virulent GBS sequence type (ST), ST485 of the clonal complex 103, has become increasingly common in China, specifically, with the frequency of isolation quickly climbing from 1% to 14% (85). These isolates have evolved from a genetic lineage capable of causing both human and bovine disease, and both the increase in virulence and rapid emergence of these isolates are thought to be due to the acquisition of the *cadDX* operon (85).

An additional strength of our study is the sensitivity of our screen to detect genes involved in overcoming various degrees of metal starvation. We identified 30 genes that were essential for GBS growth in a subinhibitory concentration of calprotectin (see Table S1 in the supplemental material), representing genes that are necessary for overcoming low-level metal sequestration but are nonessential for survival in extreme metal limitation. Genes of importance include those encoding two ribosomal proteins, key enzymes involved in glycolysis, two enzymes involved in folate metabolism, and a cobalt transporter ATPase. We also identified 55 uniquely essential genes for survival in inhibitory levels of calprotectin. These genes represent those that are important for growth when GBS encounters high degrees of starvation or the starvation of multiple metals. Systems of interest in these data were genes encoding four ribosomal proteins, six prophage-related proteins, phosphotransferase systems, and the stress response serine protease HtrA (Table S1). These differential findings are significant, as it is becoming increasingly appreciated that metal starvation/intoxication occurs across a gradient and that the maintenance of metal homeostasis is dynamic and requires numerous fine-tuned responses. These data are supported by previous studies that show streptococcal metabolism (86, 87) to be dependent on metal ions and that ribosomal proteins serve as reservoirs for intracellular zinc during metal limitation (88).

As the relative contribution of zinc homeostasis to GBS virulence had not been previously characterized, we utilized a murine model of GBS systemic infection to compare WT and Δ*adcA*Δ*adcAII*Δ*lmb* strains. These experiments demonstrated that the Δ*adcA*Δ*adcAII*Δ*lmb* mutant was significantly attenuated compared to WT GBS in two different GBS strain backgrounds and in different mouse strains. These data further validate our *in vitro* results and confirm the importance of zinc uptake machinery to the pathogenesis of GBS infection. To determine the contribution of host calprotectin to the GBS disease process, we utilized a calprotectin knockout mouse strain ($S100A9^{-/-}$) (89, 90). In contrast to the phenotypes observed in WT mice, $S100A9^{-/-}$ mice were

equally susceptible to GBS WT and Δ*adcA*Δ*adcAII*Δ*lmb* strains (Fig. 7A), suggesting that zinc transport machinery is expendable when the zinc-limiting pressure of calprotectin is absent. Furthermore, we observed that WT mice exhibited increased mortality due to GBS infection compared to that of *S100A9*$^{-/-}$ mice. In our studies, nearly 90% of WT mice infected with WT GBS succumbed to illness by 48 h, whereas the *S100A9*$^{-/-}$ mice infected with WT GBS did not reach 50% lethality until 90 h postinfection. Similar trends were recently observed in *S100A9*$^{-/-}$ mice challenged with *S. pyogenes* (91). Additionally, these data are consistent with previous findings that suggest a role for calprotectin as an immunological alarmin in promoting inflammatory signaling (92–94). Studies to determine the specific role of calprotectin in inflammation during GBS disease progression warrant further investigation.

Here, we report the generation and utilization of a highly saturated GBS *mariner* transposon library to investigate bacterial response to calprotectin-mediated metal chelation. Genome-wide screening revealed numerous metabolic pathways and metal transport systems that may contribute to the ability of GBS to overcome calprotectin stress and nutritional immunity. Our results emphasize the importance of zinc transport to the development of GBS systemic infection, highlighting the significance of zinc homeostasis to disease progression. As zinc uptake machinery is highly conserved across streptococcal pathogens, they present a promising target for the development of novel antimicrobials.

MATERIALS AND METHODS

Bacterial strains and growth conditions. *Streptococcus agalactiae* (GBS) isolates A909 (serotype Ia), CJB111 (serotype V), COH1 (serotype III), a cohort of 25 vaginal colonization isolates (serotypes Ia, Ib, II, III, and V) (49), and mutant strains (A909 Δ*adcA*, A909 Δ*adcAII*, A909 Δ*lmb*, A909 Δ*adcA*Δ*adcAII*Δ*lmb*, and CJB111 Δ*adcA*Δ*adcAII*Δ*lmb*) were cultured in Todd-Hewitt broth (THB) at 37°C. Mutant strains were constructed as previously described (40, 41). Deletion of these genes did not affect growth in metal-sufficient medium (40).

Calprotectin growth assays. Briefly, GBS cultures grown overnight (for 18 h) in THB were diluted 1:50 into 100 μl in a 96-well microtiter plate with 38% 3× modified RPMI medium (mRPMI) (95) (RPMI powder [Gibco 31800-022], 150 mM HEPES [pH 7.4], 1.5% glucose, 3× basal medium Eagle [BME] vitamins [Sigma], 75 μg/ml guanine, 75 μg/ml uracil, and 75 μg/ml adenine), 62% calprotectin buffer (20 mM Tris [pH 7.5], 100 mM NaCl, and 3 mM CaCl$_2$), and 0 to 240 μg/ml recombinant calprotectin (70, 96). The range of recombinant calprotectin was previously established for assaying bacterial survival *in vitro* (17, 97). At 8 h postinoculation, growth was assessed by measuring optical density (OD$_{600}$) and plating serial dilutions to quantitate CFU. In experiments where zinc was supplemented to counter calprotectin chelation, zinc sulfate was added at 50 μM for A909 or 100 μM for COH1 and CJB111 strains.

Generation of *mariner* (*Krmit*) mutant libraries in GBS for Tn sequencing. *In vivo mariner* transposition for random mutagenesis in GBS was accomplished using the pKrmit system originally developed for GAS (50), as previously described (50, 98). Briefly, GBS CJB111 cells were transformed by electroporation with 300 μg of pKrmit and outgrown in THY at 30°C (permissive temperature for pKrmit replication) for 4 h. Transformants were then selected by plating on THY agar containing 300 μg/ml kanamycin (Km) 100 μg/ml and spectinomycin at 30°C for 48 h. The presence of intact pKrmit was phenotypically tested as previously described (98), and proper GBS transformants were stored at −80°C. For *Krmit* transposition, an individual pKrmit-containing GBS freezer stock was used to inoculate 250 ml of THY containing Km and incubated overnight at 37°C (T$_o$) (nonpermissive temperature for pKrmit replication). The quality of *Krmit* transposition was tested as previously described (98, 99): the complexity or randomness of *Krmit* mutant libraries was assessed by amplifying the insertion sites of random mutants by arbitrarily primed PCR (AP-PCR), Sanger DNA sequencing, and mapping onto the appropriate GBS genome. Percent randomness was determined by defining a ratio of unique insertions (by AP-PCR sequencing) among a tested population.

Transposon library screening. The GBS pooled *Krmit* library was grown overnight in THB with 300 μg/ml kanamycin. Overnight culture was back diluted into 38% 3× mRPMI with 62% calprotectin buffer and 0, 60, or 480 μg/ml purified calprotectin. Samples were incubated at 37°C for 8 h. Following incubation, samples were centrifuged and resuspended in 200 μl phosphate-buffered saline (PBS). The total volume was spread onto Todd-Hewitt agar (THA) plates and incubated overnight at 37°C. Bacterial growth from each treatment condition was collected and pooled into three samples, and genomic DNA was extracted using a Zymobiomics DNA miniprep kit (Zymo Research).

Transposon library sequencing. Library preparation and sequencing were performed as previously described (51) by the microarray and genomics core at the University of Colorado Anschutz Medical Campus. Briefly, genomic DNA was sheared to approximately 340-bp fragments and processed through the Ovation Ultralow V2 DNA-Seq library preparation kit (Tecan); 9 ng of each library was used as the template to enrich by PCR (16 cycles) for the transposon insertions using *Krmit*-specific (TCGTCGGCAG CGTCAGATGTGTATAAGAGACAGCCGGGGACTTATCA<u>T</u>CCAACC) and Illumina P7 primers. The enriched PCR products were diluted 1:100, and 20 μl was used as the template for an indexing PCR (9 cycles) using

the TruSeq P5 indexing and P7 primers. Sequencing was performed using an Illumina NovaSeq 6000 in a 150-base paired-end format.

Bioinformatic analyses of Tn sequencing. Two annotated *Streptococcus agalactiae* genomes were used as the reference for these analyses, namely, CJB111 (AAJQ01000001) and A909 (NC_007432). The provided annotation is based on the A909 genome, as the annotated CJB111 genome has significantly lower coverage. Italicized directory names (ending in/) refer to directories within the git repository for this project available at https://github.com/abelew/sagalacticae_2019. Much of the postprocessing was handled by the hpgltools R package (100). Approximately 2.5 million reads of each raw library were queried for quality with Fastqc (101) before removing the *mariner* inverted terminal repeat (ITR) leading sequences with cutadapt (102). These libraries were aligned against the reference genomes with Bowtie (103, 104) using options to allow one mismatch (-v 1) and randomly assign multimatched reads to one of the possible matching positions (-M 1). The resulting alignments were converted to sorted/compressed binary alignments (105) and counted (106) against the reference genome coding DNA sequence (CDS) and intergenic regions. The essentiality software package (52) provides an opportunity to query statistically significant stretches of TAs that have no observed insertions to further inform its metric of essentiality. The insertion data were therefore converted into its expected format and passed to the version 1.21 of the implementation Python script. The resulting table provided a count of the number of insertions observed in each open reading frame (ORF), the number of observed TAs, the maximum length of the nonobserved sequence, the nucleotide span of this region, a call on whether each ORF is essential, and the posterior probability for each call. The default options were used, except multiple runs were performed with the minimum hit parameter set to 1, 2, 4, 8, 16, and 32. These operations were performed via CYOA (https://github.com/abelew/CYOA). In a separate invocation, the three replicates for the control, low concentration, and high concentration samples were concatenated into a single sample, and essentiality was run on the combined samples. The libraries were quantified with respect to relative coverage, similarity, and saturation and with respect to available TA insertion points. These tasks were performed using the hpgltools and the input text/wig files for the essentiality package. Thus, the essentiality input files were read into the R function "plot_saturation" and used to visualize the saturation of each library. This was done by taking the $\log_2$ (hits + 1) for each position and plotting them as a set of histograms. Comparison and normalization of control (input) and experimental (output) libraries were performed similarly to the essentials software package (107, 108) but using a combination of voom/limma, EdgeR, DESeq2, EBSeq, and a statistically uninformed basic analysis instead of EdgeR. Pairwise Euclidean distances, Spearman correlation coefficients, and principal-component analyses were then used to visualize the similarities/differences between normalized libraries. Clustering of orthologous groups of proteins (COGs) were assigned using EggNOG 5.0.0 (109), and Venn diagrams were calculated and plotted using BxToolBox (BioInfoRx, Inc., Madison, WI).

Quantitative reverse transcriptase PCR (qRT-PCR) and ELISA. GBS strains were grown to mid-logarithmic phase (OD_{600} of 0.4) in mRPMI and incubated with 120 μg/ml calprotectin for 1 h at 37°C or 25 μm TPEN for 15 min at 37°C. Following incubation, bacteria were centrifuged at 5,000 $\times$ g for 5 min, total RNA was extracted (Macherey-Nagel), and cDNA was synthesized (Quanta Biosciences) per the manufacturers' instructions. The following primer sequences (shown 5' to 3') were used in this study: *adcA* (forward [F], GAACGTGCGATTTCTGTTGTAG; reverse [R], TGCAATGTAAGCATCTGCATTT), *adcAII* (F, GCTAGTTGTGTAGCGATGAGTT; R, GGAGTAGATGAGTCAACCTTGTATG), *lmb* (F, GGCCTGGAAGATATGGAA GTG; R, GTATGCTGGGTCACAAAGGT), and *czcD* (F, TCAATACCATCCATTGACCAGAT; R, GATTCCATAGATT ACGCTGCATTAC). KC from mouse brain homogenates was quantitated by enzyme-linked immunosorbent assay (ELISA) per the manufacturer's instructions (R&D Systems).

Ortholog clustering. To evaluate if metal transport machinery involved in survival during calprotectin stress was orthologous to that in characterized systems, the closely related *Streptococcus pneumoniae* TIGR4 (GCF_000006885.1) and *S. agalactiae* A909 (GCF_000012705.1) were used as input for the program OrthoFinder v. 2.2.6 (110). Domain architecture of proteins in each orthogroup collected were evaluated using InterProScan v. 5.27-66.0 (111). Predicted operons in GBS were determined using the Database of prOkaryotic OpeRons (DOOR²) (112–114).

Mouse model of GBS systemic infection. All animal experiments were conducted under the approval of the Institutional Animal Care and Use Committee (number 00316) at the University of Colorado Anschutz Medical Campus and performed using accepted veterinary standards. We utilized a mouse model of systemic infection as previously described (28, 36, 37), in which female 8-week-old C57BL/6, C57BL/6 *S100A9*$^{-/-}$, and CD1 mice were injected intravenously with 3 $\times$ 10⁸ CFU of WT A909 or A909 Δ*adcA*Δ*adcAII*Δ*lmb* or 1 $\times$ 10⁷ CFU CJB111 or CJB111 Δ*adcA*Δ*adcAII*Δ*lmb* mutant strains. Mice were euthanized, and blood and brain tissues were collected. Tissue homogenates and blood were plated on THA to quantify GBS CFU burden.

Statistical analyses. Significance during calprotectin growth experiments was determined by the Kruskal-Wallis test with Dunn's multiple-comparison posttest with treated samples compared to untreated controls. Normality was confirmed for clinical isolate data by the Shapiro-Wilk test, and significance was determined by one-way analysis of variance (ANOVA) with Tukey's multiple-comparison posttest. Calprotectin growth assays using GBS WT and mutant strains was analyzed by the Kruskal-Wallis test with Dunnett's multiple-comparison test. Statistical differences in murine experiments were determined by the log rank Mantel-Cox test for survival and by an unpaired Student's t test. Statistical significance was accepted when P value was $<\alpha$, with an α of 0.05.

Data availability. Sequencing reads from the transposon sequencing analyses are available in the NCBI Sequence Read Archive (SRA) under the accession number PRJNA667098.

SUPPLEMENTAL MATERIAL

Supplemental material is available online only.

FIG S1, TIF file, 0.1 MB.

FIG S2, TIF file, 0.2 MB.

FIG S3, TIF file, 0.2 MB.

TABLE S1, XLSX file, 0.4 MB.

ACKNOWLEDGMENTS

REFERENCES

1. Andreini C, Bertini I, Cavallaro G, Holliday GL, Thornton JM. 2008. Metal ions in biological catalysis: from enzyme databases to general principles. J Biol Inorg Chem 13:1205–1218. https://doi.org/10.1007/s00775-008-0404-5.

2. Zygiel EM, Nolan EM. 2018. Transition metal sequestration by the host-defense protein calprotectin. Annu Rev Biochem 87:621–643. https://doi.org/10.1146/annurev-biochem-062917-012312.

3. Waldron KJ, Robinson NJ. 2009. How do bacterial cells ensure that metalloproteins get the correct metal? Nat Rev Microbiol 7:25–35. https://doi.org/10.1038/nrmicro2057.

4. Waldron KJ, Rutherford JC, Ford D, Robinson NJ. 2009. Metalloproteins and metal sensing. Nature 460:823–830. https://doi.org/10.1038/nature08300.

5. Hood MI, Skaar EP. 2012. Nutritional immunity: transition metals at the pathogen-host interface. Nat Rev Microbiol 10:525–537. https://doi.org/10.1038/nrmicro2836.

6. Becker KW, Skaar EP. 2014. Metal limitation and toxicity at the interface between host and pathogen. FEMS Microbiol Rev 38:1235–1249. https://doi.org/10.1111/1574-6976.12087.

7. Corbin BD, Seeley EH, Raab A, Feldmann J, Miller MR, Torres VJ, Anderson KL, Dattilo BM, Dunman PM, Gerads R, Caprioli RM, Nacken W, Chazin WJ, Skaar EP. 2008. Metal chelation and inhibition of bacterial growth in tissue abscesses. Science 319:962–965. https://doi.org/10.1126/science.1152449.

8. Hood MI, Mortensen BL, Moore JL, Zhang Y, Kehl-Fie TE, Sugitani N, Chazin WJ, Caprioli RM, Skaar EP. 2012. Identification of an *Acinetobacter baumannii* zinc acquisition system that facilitates resistance to calprotectin-mediated zinc sequestration. PLoS Pathog 8:e1003068. https://doi.org/10.1371/journal.ppat.1003068.

9. Achouiti A, Vogl T, Urban CF, Röhm M, Hommes TJ, van Zoelen MAD, Florquin S, Roth J, van 't Veer C, de Vos AF, van der Poll T. 2012. Myeloid-related protein-14 contributes to protective immunity in Gram-negative pneumonia-derived sepsis. PLoS Pathog 8:e1002987. https://doi.org/10.1371/journal.ppat.1002987.

10. Weinberg ED. 1975. Nutritional immunity: host's attempt to withhold iron from microbial invaders. JAMA 231:39–41. https://doi.org/10.1001/jama.1975.03240130021018.

11. Xiao X, Yeoh BS, Vijay-Kumar M. 2017. Lipocalin 2: an emerging player in iron homeostasis and inflammation. Annu Rev Nutr 37:103–130. https://doi.org/10.1146/annurev-nutr-071816-064559.

12. Cassat JE, Skaar EP. 2013. Iron in infection and immunity. Cell Host Microbe 13:509–519. https://doi.org/10.1016/j.chom.2013.04.010.

13. Kehl-Fie TE, Skaar EP. 2010. Nutritional immunity beyond iron: a role for manganese and zinc. Curr Opin Chem Biol 14:218–224. https://doi.org/10.1016/j.cbpa.2009.11.008.

14. Brophy MB, Hayden JA, Nolan EM. 2012. Calcium ion gradients modulate the zinc affinity and antibacterial activity of human calprotectin. J Am Chem Soc 134:18089–18100. https://doi.org/10.1021/ja307974e.

15. Nakashige TG, Stephan JR, Cunden LS, Brophy MB, Wommack AJ, Keegan BC, Shearer JM, Nolan EM. 2016. The hexahistidine motif of host-defense protein human calprotectin contributes to zinc withholding and its functional versatility. J Am Chem Soc 138:12243–12251. https://doi.org/10.1021/jacs.6b06845.

16. Hayden JA, Brophy MB, Cunden LS, Nolan EM. 2013. High-affinity manganese coordination by human calprotectin is calcium-dependent and requires the histidine-rich site formed at the dimer interface. J Am Chem Soc 135:775–787. https://doi.org/10.1021/ja3096416.

17. Kehl-Fie TE, Chitayat S, Hood MI, Damo S, Restrepo N, Garcia C, Munro KA, Chazin WJ, Skaar EP. 2011. Nutrient metal sequestration by calprotectin inhibits bacterial superoxide defense, enhancing neutrophil killing of *Staphylococcus aureus*. Cell Host Microbe 10:158–164. https://doi.org/10.1016/j.chom.2011.07.004.

18. Nakashige TG, Zhang B, Krebs C, Nolan EM. 2015. Human calprotectin is an iron-sequestering host-defense protein. Nat Chem Biol 11:765–771. https://doi.org/10.1038/nchembio.1891.

19. Zygiel EM, Nelson CE, Brewer LK, Oglesby-Sherrouse AG, Nolan EM. 2019. The human innate immune protein calprotectin induces iron starvation responses in *Pseudomonas aeruginosa*. J Biol Chem 294:3549–3562. https://doi.org/10.1074/jbc.RA118.006819.

20. Wang J, Lonergan ZR, Gonzalez-Gutierrez G, Nairn BL, Maxwell CN, Zhang Y, Andreini C, Karty JA, Chazin WJ, Trinidad JC, Skaar EP, Giedroc DP. 2019. Multi-metal restriction by calprotectin impacts *de novo* flavin biosynthesis in *Acinetobacter baumannii*. Cell Chem Biol 26:745.e7–755.e7. https://doi.org/10.1016/j.chembiol.2019.02.011.

21. Besold AN, Gilston BA, Radin JN, Ramsoomair C, Culbertson EM, Li CX, Cormack BP, Chazin WJ, Kehl-Fie TE, Culotta VC. 2017. Role of calprotectin in withholding zinc and copper from *Candida albicans*. Infect Immun 86:e00779-17. https://doi.org/10.1128/IAI.00779-17.

22. Nakashige TG, Zygiel EM, Drennan CL, Nolan EM. 2017. Nickel sequestration by the host-defense protein human calprotectin. J Am Chem Soc 139:8828–8836. https://doi.org/10.1021/jacs.7b01212.

23. Vernia F, Di Ruscio M, Stefanelli G, Viscido A, Frieri G, Latella G. 2020. Is fecal calprotectin an accurate marker in the management of Crohn's disease? J Gastroenterol Hepatol 35:390–400. https://doi.org/10.1111/jgh.14950.

24. National Institute for Health and Care Excellence. 2013. Faecal calprotectin diagnostic tests for inflammatory diseases of the bowel. Diagnostics guidance [DG11]. National Institute for Health and Care Excellence, London, United Kingdom.

25. Gebhardt C, Németh J, Angel P, Hess J. 2006. S100a8 and S100a9 in inflammation and cancer. Biochem Pharmacol 72:1622–1631. https://doi.org/10.1016/j.bcp.2006.05.017.

26. Schuchat A. 1999. Group B *Streptococcus*. Lancet 353:51–56. https://doi.org/10.1016/S0140-6736(98)07128-1.

27. Ferrieri P, Burke B, Nelson J. 1980. Production of bacteremia and meningitis in infant rats with group B streptococcal serotypes. Infect Immun 27:1023–1032. https://doi.org/10.1128/IAI.27.3.1023-1032.1980.

28. Doran KS, Engelson EJ, Khosravi A, Maisey HC, Fedtke I, Equils O, Michelsen KS, Arditi M, Peschel A, Nizet V. 2005. Blood-brain barrier invasion by group B *Streptococcus* depends upon proper cell-surface

anchoring of lipoteichoic acid. J Clin Invest 115:2499–2507. https://doi.org/10.1172/JCI23829.

29. Melin P. 2011. Neonatal group B streptococcal disease: from pathogenesis to preventive strategies. Clin Microbiol Infect 17:1294–1303. https://doi.org/10.1111/j.1469-0691.2011.03576.x.

30. CDC. 2017. Active bacterial surveillance report, Emerging Infections Program Network, group B Streptococcus. Centers for Disease Control and Prevention, Atlanta, GA.

31. Epstein FH, Quagliariello V, Scheld WM. 1992. Bacterial meningitis: pathogenesis, pathophysiology, and progress. N Engl J Med 327:864–872. https://doi.org/10.1056/NEJM199209173271208.

32. Bundy LM, Noor A. 2020. Neonatal meningitis. StatPearls Publishing, Treasure Island, FL.

33. Libster R, Edwards KM, Levent F, Edwards MS, Rench MA, Castagnini LA, Cooper T, Sparks RC, Baker CJ, Shah PE. 2012. Long-term outcomes of group B streptococcal meningitis. Pediatrics 130:e8–e15. https://doi.org/10.1542/peds.2011-3453.

34. Gordon SM, Srinivasan L, Harris MC. 2017. Neonatal meningitis: overcoming challenges in diagnosis, prognosis, and treatment with omics. Front Pediatr 5:139. https://doi.org/10.3389/fped.2017.00139.

35. Doran KS, Chang JCW, Benoit VM, Eckmann L, Nizet V. 2002. Group B streptococcal ß-hemolysin/cytolysin promotes invasion of human lung epithelial cells and the release of interleukin-8. J Infect Dis 185:196–203. https://doi.org/10.1086/338475.

36. Banerjee A, Kim BJ, Carmona EM, Cutting AS, Gurney MA, Carlos C, Feuer R, Prasadarao NV, Doran KS. 2011. Bacterial pili exploit integrin machinery to promote immune activation and efficient blood-brain barrier penetration. Nat Commun 2:462. https://doi.org/10.1038/ncomms1474.

37. Deng L, Spencer BL, Holmes JA, Mu R, Rego S, Weston TA, Hu Y, Sanches GF, Yoon S, Park N, Nagao PE, Jenkinson HF, Thornton JA, Seo KS, Nobbs AH, Doran KS. 2019. The group B streptococcal surface antigen I/Ii protein, Bspc, interacts with host vimentin to promote adherence to brain endothelium and inflammation during the pathogenesis of meningitis. PLoS Pathog 15:e1007848. https://doi.org/10.1371/journal.ppat.1007848.

38. Kothary V, Doster RS, Rogers LM, Kirk LA, Boyd KL, Romano-Keeler J, Haley KP, Manning SD, Aronoff DM, Gaddy JA. 2017. Group B Streptococcus induces neutrophil recruitment to gestational tissues and elaboration of extracellular traps and nutritional immunity. Front Cell Infect Microbiol 7:19. https://doi.org/10.3389/fcimb.2017.00019.

39. Gravett MG. 2004. Diagnosis of intra-amniotic infection by proteomic profiling and identification of novel biomarkers. JAMA 292:462. https://doi.org/10.1001/jama.292.4.462.

40. Moulin P, Patron K, Cano C, Zorgani MA, Camiade E, Borezée-Durant E, Rosenau A, Mereghetti L, Hiron A. 2016. The Adc/Lmb system mediates zinc acquisition in Streptococcus agalactiae and contributes to bacterial growth and survival. J Bacteriol 198:3265–3277. https://doi.org/10.1128/JB.00614-16.

41. Moulin P, Rong V, Ribeiro E Silva A, Pederick VG, Camiade E, Mereghetti L, McDevitt CA, Hiron A. 2019. Defining the role of the Streptococcus agalactiae Sht-family proteins in zinc acquisition and complement evasion. J Bacteriol 201:e00757-18. https://doi.org/10.1128/JB.00757-18.

42. Bayle L, Chimalapati S, Schoehn G, Brown J, Vernet T, Durmort C. 2011. Zinc uptake by Streptococcus pneumoniae depends on both AdcA and AdcAII and is essential for normal bacterial morphology and virulence. Mol Microbiol 82:904–916. https://doi.org/10.1111/j.1365-2958.2011.07862.x.

43. Plumptre CD, Eijkelkamp BA, Morey JR, Behr F, Couñago RM, Ogunniyi AD, Kobe B, O'Mara ML, Paton JC, McDevitt CA. 2014. AdcA and AdcAII employ distinct zinc acquisition mechanisms and contribute additively to zinc homeostasis in Streptococcus pneumoniae. Mol Microbiol 91:834–851. https://doi.org/10.1111/mmi.12504.

44. Brown LR, Gunnell SM, Cassella AN, Keller LE, Scherkenbach LA, Mann B, Brown MW, Hill R, Fitzkee NC, Rosch JW, Tuomanen EI, Thornton JA. 2016. AdcAII of Streptococcus pneumoniae affects pneumococcal invasiveness. PLoS One 11:e0146785. https://doi.org/10.1371/journal.pone.0146785.

45. Tedde V, Rosini R, Galeotti CL. 2016. Zn²⁺ uptake in Streptococcus pyogenes: characterization of adcA and lmb null mutants. PLoS One 11:e0152835. https://doi.org/10.1371/journal.pone.0152835.

46. Madoff LC, Michel JL, Kasper DL. 1991. A monoclonal antibody identifies a protective C-protein alpha-antigen epitope in group B streptococci. Infect Immun 59:204–210. https://doi.org/10.1128/IAI.59.1.204-210.1991.

47. Faralla C, Metruccio MM, De Chiara M, Mu R, Patras KA, Muzzi A, Grandi G, Margarit I, Doran KS, Janulczyk R. 2014. Analysis of two-component systems in group B Streptococcus shows that RgfAC and the novel FspSR modulate virulence and bacterial fitness. mBio 5:e00870-14. https://doi.org/10.1128/mBio.00870-14.

48. Wilson CB, Weaver WM. 1985. Comparative susceptibility of group B streptococci and Staphylococcus aureus to killing by oxygen metabolites. J Infect Dis 152:323–329. https://doi.org/10.1093/infdis/152.2.323.

49. Burcham LR, Spencer BL, Keeler LR, Runft DL, Patras KA, Neely MN, Doran KS. 2019. Determinants of group B streptococcal virulence potential amongst vaginal clinical isolates from pregnant women. PLoS One 14:e0226699. https://doi.org/10.1371/journal.pone.0226699.

50. Le Breton Y, Belew AT, Valdes KM, Islam E, Curry P, Tettelin H, Shirtliff ME, El-Sayed NM, McIver KS. 2015. Essential genes in the core genome of the human pathogen Streptococcus pyogenes. Sci Rep 5:9838. https://doi.org/10.1038/srep09838.

51. Dale JL, Beckman KB, Willett JLE, Nilson JL, Palani NP, Baller JA, Hauge A, Gohl DM, Erickson R, Manias DA, Sadowsky MJ, Dunny GM. 2018. Comprehensive functional analysis of the Enterococcus faecalis core genome using an ordered, sequence-defined collection of insertional mutations in strain OG1RF. mSystems 3:e00062-18. https://doi.org/10.1128/mSystems.00062-18.

52. DeJesus MA, Zhang YJ, Sassetti CM, Rubin EJ, Sacchettini JC, Ioerger TR. 2013. Bayesian analysis of gene essentiality based on sequencing of transposon insertion libraries. Bioinformatics 29:695–703. https://doi.org/10.1093/bioinformatics/btt043.

53. Bray BA, Sutcliffe IC, Harrington DJ. 2009. Expression of the MtsA lipoprotein of Streptococcus agalactiae A909 is regulated by manganese and iron. Antonie Van Leeuwenhoek 95:101–109. https://doi.org/10.1007/s10482-008-9291-6.

54. Eijkelkamp BA, McDevitt CA, Kitten T. 2015. Manganese uptake and streptococcal virulence. Biometals 28:491–508. https://doi.org/10.1007/s10534-015-9826-z.

55. Rosch JW, Gao G, Ridout G, Wang Y-D, Tuomanen EI. 2009. Role of the manganese efflux system mnte for signalling and pathogenesis in Streptococcus pneumoniae. Mol Microbiol 72:12–25. https://doi.org/10.1111/j.1365-2958.2009.06638.x.

56. Janulczyk R, Ricci S, Björck L. 2003. MtsABC is important for manganese and iron transport, oxidative stress resistance, and virulence of Streptococcus pyogenes. Infect Immun 71:2656–2664. https://doi.org/10.1128/IAI.71.5.2656-2664.2003.

57. Shabayek S, Bauer R, Mauerer S, Mizaikoff B, Spellerberg B. 2016. A streptococcal NRAMP homologue is crucial for the survival of Streptococcus agalactiae under low pH conditions. Mol Microbiol 100:589–606. https://doi.org/10.1111/mmi.13335.

58. Nemec AA, Leikauf GD, Pitt BR, Wasserloos KJ, Barchowsky A. 2009. Nickel mobilizes intracellular zinc to induce metallothionein in human airway epithelial cells. Am J Respir Cell Mol Biol 41:69–75. https://doi.org/10.1165/rcmb.2008-0409OC.

59. Arslan P, Di Virgilio F, Beltrame M, Tsien RY, Pozzan T. 1985. Cytosolic Ca²⁺ homeostasis in Ehrlich and Yoshida carcinomas. A new, membrane-permeant chelator of heavy metals reveals that these ascites tumor cell lines have normal cytosolic free Ca²⁺. J Biol Chem 260:2719–2727.

60. Hyun HJ, Sohn JH, Ha DW, Ahn YH, Koh JY, Yoon YH. 2001. Depletion of intracellular zinc and copper with TPEN results in apoptosis of cultured human retinal pigment epithelial cells. Invest Ophthalmol Vis Sci 42:460–465.

61. Wennekamp J, Henneke P. 2008. Induction and termination of inflammatory signaling in group B streptococcal sepsis. Immunol Rev 225:114–127. https://doi.org/10.1111/j.1600-065X.2008.00673.x.

62. Røseth AG, Aadland E, Jahnsen J, Raknerud N. 1997. Assessment of disease activity in ulcerative colitis by faecal calprotectin, a novel granulocyte marker protein. Digestion 58:176–180. https://doi.org/10.1159/000201441.

63. Urban CF, Ermert D, Schmid M, Abu-Abed U, Goosmann C, Nacken W, Brinkmann V, Jungblut PR, Zychlinsky A. 2009. Neutrophil extracellular traps contain calprotectin, a cytosolic protein complex involved in host defense against Candida albicans. PLoS Pathog 5:e1000639. https://doi.org/10.1371/journal.ppat.1000639.

64. Hooven TA, Catomeris AJ, Akabas LH, Randis TM, Maskell DJ, Peters SE, Ott S, Santana-Cruz I, Tallon LJ, Tettelin H, Ratner AJ. 2016. The essential

genome of *Streptococcus agalactiae*. BMC Genomics 17:406. https://doi.org/10.1186/s12864-016-2741-z.

65. Caymaris S, Bootsma HJ, Martin B, Hermans PWM, Prudhomme M, Claverys J-P. 2010. The global nutritional regulator CodY is an essential protein in the human pathogen *Streptococcus pneumoniae*. Mol Microbiol 78:344–360. https://doi.org/10.1111/j.1365-2958.2010.07339.x.

66. Blindauer CA. 2015. Advances in the molecular understanding of biological zinc transport. Chem Commun (Camb) 51:4544–4563. https://doi.org/10.1039/C4CC10174J.

67. Capdevila DA, Wang J, Giedroc DP. 2016. Bacterial strategies to maintain zinc metallostasis at the host-pathogen interface. J Biol Chem 291:20858–20868. https://doi.org/10.1074/jbc.R116.742023.

68. Mikhaylina A, Ksibe AZ, Scanlan DJ, Blindauer CA. 2018. Bacterial zinc uptake regulator proteins and their regulons. Biochem Soc Trans 46:983–1001. https://doi.org/10.1042/BST20170228.

69. Kandari D, Gopalani M, Gupta M, Joshi H, Bhatnagar S, Bhatnagar R. 2018. Identification, functional characterization, and regulon prediction of the zinc uptake regulator (Zur) of *Bacillus anthracis* – an insight into the zinc homeostasis of the pathogen. Front Microbiol 9:3314. https://doi.org/10.3389/fmicb.2018.03314.

70. Grim KP, San Francisco B, Radin JN, Brazel EB, Kelliher JL, Párraga Solórzano PK, Kim PC, McDevitt CA, Kehl-Fie TE. 2017. The metallophore staphylopine enables *Staphylococcus aureus* to compete with the host for zinc and overcome nutritional immunity. mBio 8:e01281-17. https://doi.org/10.1128/mBio.01281-17.

71. Dintilhac A, Alloing G, Granadel C, Claverys JP. 1997. Competence and virulence of *Streptococcus pneumoniae*: Adc and PsaA mutants exhibit a requirement for Zn and Mn resulting from inactivation of putative ABC metal permeases. Mol Microbiol 25:727–739. https://doi.org/10.1046/j.1365-2958.1997.5111879.x.

72. Lindahl G, Stålhammar-Carlemalm M, Areschoug T. 2005. Surface proteins of *Streptococcus agalactiae* and related proteins in other bacterial pathogens. Clin Microbiol Rev 18:102–127. https://doi.org/10.1128/CMR.18.1.102-127.2005.

73. Elsner A, Kreikemeyer B, Braun-Kiewnick A, Spellerberg B, Buttaro BA, Podbielski A. 2002. Involvement of Lsp, a member of the Lral-lipoprotein family in *Streptococcus pyogenes*, in eukaryotic cell adhesion and internalization. Infect Immun 70:4859–4869. https://doi.org/10.1128/IAI.70.9.4859-4869.2002.

74. Spellerberg B, Rozdzinski E, Martin S, Weber-Heynemann J, Schnitzler N, Lütticken R, Podbielski A. 1999. Lmb, a protein with similarities to the Lral adhesin family, mediates attachment of *Streptococcus agalactiae* to human laminin. Infect Immun 67:871–878. https://doi.org/10.1128/IAI.67.2.871-878.1999.

75. Terao Y, Kawabata S, Kunitomo E, Nakagawa I, Hamada S. 2002. Novel laminin-binding protein of *Streptococcus pyogenes*, Lbp, is involved in adhesion to epithelial cells. Infect Immun 70:993–997. https://doi.org/10.1128/IAI.70.2.993-997.2002.

76. Cook LCC, Hu H, Maienschein-Cline M, Federle MJ. 2018. A vaginal tract signal detected by the group B *Streptococcus* SaeRS system elicits transcriptomic changes and enhances murine colonization. Infect Immun 86:e00762-17. https://doi.org/10.1128/IAI.00762-17.

77. Mereghetti L, Sitkiewicz I, Green NM, Musser JM. 2008. Extensive adaptive changes occur in the transcriptome of *Streptococcus agalactiae* (group B *Streptococcus*) in response to incubation with human blood. PLoS One 3:e3143. https://doi.org/10.1371/journal.pone.0003143.

78. Jean S, Juneau RA, Criss AK, Cornelissen CN. 2016. *Neisseria gonorrhoeae* evades calprotectin-mediated nutritional immunity and survives neutrophil extracellular traps by production of TdfH. Infect Immun 84:2982–2994. https://doi.org/10.1128/IAI.00319-16.

79. Tettelin H, Masignani V, Cieslewicz MJ, Donati C, Medini D, Ward NL, Angiuoli SV, Crabtree J, Jones AL, Durkin AS, Deboy RT, Davidsen TM, Mora M, Scarselli M, Margarit y Ros I, Peterson JD, Hauser CR, Sundaram JP, Nelson WC, Madupu R, Brinkac LM, Dodson RJ, Rosovitz MJ, Sullivan SA, Daugherty SC, Haft DH, Selengut J, Gwinn ML, Zhou L, Zafar N, Khouri H, Radune D, Dimitrov G, Watkins K, O'Connor KJB, Smith S, Utterback TR, White O, Rubens CE, Grandi G, Madoff LC, Kasper DL, Telford JL, Wessels MR, Rappuoli R, Fraser CM. 2005. Genome analysis of multiple pathogenic isolates of *Streptococcus agalactiae*: implications for the microbial "pan-genome". Proc Natl Acad Sci U S A 102:13950–13955. https://doi.org/10.1073/pnas.0506758102.

80. Martin JE, Edmonds KA, Bruce KE, Campanello GC, Eijkelkamp BA, Brazel EB, McDevitt CA, Winkler ME, Giedroc DP. 2017. The zinc efflux activator SczA protects *Streptococcus pneumoniae* serotype 2 D39 from

intracellular zinc toxicity. Mol Microbiol 104:636–651. https://doi.org/10.1111/mmi.13654.

81. Ong CL, Gillen CM, Barnett TC, Walker MJ, McEwan AG. 2014. An antimicrobial role for zinc in innate immune defense against group A *Streptococcus*. J Infect Dis 209:1500–1508. https://doi.org/10.1093/infdis/jiu053.

82. Martin JE, Giedroc DP. 2016. Functional determinants of metal ion transport and selectivity in paralogous cation diffusion facilitator transporters CzcD and MntE in *Streptococcus pneumoniae*. J Bacteriol 198:1066–1076. https://doi.org/10.1128/JB.00975-15.

83. Kloosterman TG, van der Kooi-Pol MM, Bijlsma JJE, Kuipers OP. 2007. The novel transcriptional regulator SczA mediates protection against Zn^{2+} stress by activation of the Zn^{2+}-resistance gene *czcD* in *Streptococcus pneumoniae*. Mol Microbiol 65:1049–1063. https://doi.org/10.1111/j.1365-2958.2007.05849.x.

84. Chen Y-YM, Feng CW, Chiu CF, Burne RA. 2008. *cadDX* operon of *Streptococcus salivarius* 57.I. Appl Environ Microbiol 74:1642–1645. https://doi.org/10.1128/AEM.01878-07.

85. Wang R, Li L, Huang T, Huang Y, Huang W, Yang X, Lei A, Chen M. 2018. Phylogenetic, comparative genomic and structural analyses of human *Streptococcus agalactiae* ST485 in China. BMC Genomics 19:716. https://doi.org/10.1186/s12864-018-5084-0.

86. Jordan MR, Wang J, Capdevila DA, Giedroc DP. 2020. Multi-metal nutrient restriction and crosstalk in metallostasis systems in microbial pathogens. Curr Opin Microbiol 55:17–25. https://doi.org/10.1016/j.mib.2020.01.010.

87. Ong C-l. Y, Walker MJ, McEwan AG. 2015. Zinc disrupts central carbon metabolism and capsule biosynthesis in *Streptococcus pyogenes*. Sci Rep 5:10799. https://doi.org/10.1038/srep10799.

88. Chandrangsu P, Huang X, Gaballa A, Helmann JD. 2019. *Bacillus subtilis* FolE is sustained by the ZagA zinc metallochaperone and the alarmone ZTP under conditions of zinc deficiency. Mol Microbiol 112:751–765. https://doi.org/10.1111/mmi.14314.

89. Vogl T, Tenbrock K, Ludwig S, Leukert N, Ehrhardt C, van Zoelen MAD, Nacken W, Foell D, van der Poll T, Sorg C, Roth J. 2007. Mrp8 and Mrp14 are endogenous activators of Toll-like receptor 4, promoting lethal, endotoxin-induced shock. Nat Med 13:1042–1049. https://doi.org/10.1038/nm1638.

90. Kuipers MT, Vogl T, Aslami H, Jongsma G, van den Berg E, Vlaar APJ, Roelofs JJTH, Juffermans NP, Schultz MJ, van der Poll T, Roth J, Wieland CW. 2013. High levels of S100A8/A9 proteins aggravate ventilator-induced lung injury via TLR4 signaling. PLoS One 8:e68694. https://doi.org/10.1371/journal.pone.0068694.

91. Makthal N, Do H, Wendel BM, Olsen RJ, Helmann JD, Musser JM, Kumaraswami M. 2020. Group A *Streptococcus* AdcR regulon participates in bacterial defense against host-mediated zinc sequestration and contributes to virulence. Infect Immun 88:e00097-20. https://doi.org/10.1128/IAI.00097-20.

92. Pittman K, Kubes P. 2013. Damage-associated molecular patterns control neutrophil recruitment. J Innate Immun 5:315–323. https://doi.org/10.1159/000347132.

93. Boyapati RK, Rossi AG, Satsangi J, Ho G-T. 2016. Gut mucosal DAMPs in IBD: from mechanisms to therapeutic implications. Mucosal Immunol 9:567–582. https://doi.org/10.1038/mi.2016.14.

94. Vandal K, Rouleau P, Boivin A, Ryckman C, Talbot M, Tessier PA. 2003. Blockade of S100A8 and S100A9 suppresses neutrophil migration in response to lipopolysaccharide. J Immunol 171:2602–2609. https://doi.org/10.4049/jimmunol.171.5.2602.

95. Edgar RJ, van Hensbergen VP, Ruda A, Turner AG, Deng P, Le Breton Y, El-Sayed NM, Belew AT, McIver KS, McEwan AG, Morris AJ, Lambeau G, Walker MJ, Rush JS, Korotkov KV, Widmalm G, van Sorge NM, Korotkova N. 2019. Discovery of glycerol phosphate modification on streptococcal rhamnose polysaccharides. Nat Chem Biol 15:463–471. https://doi.org/10.1038/s41589-019-0251-4.

96. Radin JN, Zhu J, Brazel EB, McDevitt CA, Kehl-Fie TE. 2018. Synergy between nutritional immunity and independent host defenses contributes to the importance of the MntABC manganese transporter during *Staphylococcus aureus* infection. Infect Immun 87:e00642-18. https://doi.org/10.1128/IAI.00642-18.

97. Kehl-Fie TE, Zhang Y, Moore JL, Farrand AJ, Hood MI, Rathi S, Chazin WJ, Caprioli RM, Skaar EP. 2013. MntABC and MntH contribute to systemic *Staphylococcus aureus* infection by competing with calprotectin for nutrient manganese. Infect Immun 81:3395–3405. https://doi.org/10.1128/IAI.00420-13.

98. Le Breton Y, McIver KS. 2013. Genetic manipulation of *Streptococcus pyogenes* (the group A *Streptococcus*, GAS. Curr Protoc Microbiol 30: 9D.3.1–9D.3.29. https://doi.org/10.1002/9780471729259.mc09d03s30.

99. Le Breton Y, Mistry P, Valdes KM, Quigley J, Kumar N, Tettelin H, McIver KS. 2013. Genome-wide identification of genes required for fitness of group A *Streptococcus* in human blood. Infect Immun 81:862–875. https://doi.org/10.1128/IAI.00837-12.

100. R Core Team. 2013. R: a language and environment for statistical computing. R Foundation for Statistical Computing, Vienna, Austria.

101. Andrews S. 2010. Fastqc: a quality control tool for high throughput sequence data. Babraham Bioinformatics, Babraham Institute, Cambridge, United Kingdom.

102. Martin M. 2011. Cutadapt removes adapter sequences from high-throughput sequencing reads. EMBnet J 17:10–12. https://doi.org/10.14806/ej.17.1.200.

103. Langmead B. 2010. Aligning short sequencing reads with Bowtie. Curr Protoc Bioinformatics 32:Unit 11.7. https://doi.org/10.1002/0471250953.bi1107s32.

104. Langmead B, Trapnell C, Pop M, Salzberg SL. 2009. Ultrafast and memory-efficient alignment of short DNA sequences to the human genome. Genome Biol 10:R25. https://doi.org/10.1186/gb-2009-10-3-r25.

105. Li H, Handsaker B, Wysoker A, Fennell T, Ruan J, Homer N, Marth G, Abecasis G, Durbin R, 1000 Genome Project Data Processing Subgroup. 2009. The Sequence Alignment/Map format and SAMtools. Bioinformatics 25:2078–2079. https://doi.org/10.1093/bioinformatics/btp352.

106. Anders S, Pyl PT, Hyber W. 2015. A Python framework to work with high-throughput sequencing data. Bioinformatics 31:166–169. https://doi.org/10.1093/bioinformatics/btu638.

107. Dillies M-A, Rau A, Aubert J, Hennequet-Antier C, Jeanmougin M, Servant N, Keime C, Marot G, Castel D, Estelle J, Guernec G, Jagla B, Jouneau L, Laloe D, Le Gall C, Schaeffer B, Le Crom S, Guedj M, Jaffrezic F, French StatOmique Consortium. 2013. A comprehensive evaluation of normalization methods for Illumina high-throughput RNA sequencing data analysis. Brief Bioinform 14:671–683. https://doi.org/10.1093/bib/bbs046.

108. Zomer A, Burghout P, Bootsma HJ, Hermans PWM, van Hijum SAFT. 2012. Essentials: software for rapid analysis of high throughput transposon insertion sequencing data. PLoS One 7:e43012. https://doi.org/10.1371/journal.pone.0043012.

109. Huerta-Cepas J, Szklarczyk D, Heller D, Hernández-Plaza A, Forslund SK, Cook H, Mende DR, Letunic I, Rattei T, Jensen LJ, von Mering C, Bork P. 2019. EggNOG 5.0: a hierarchical, functionally and phylogenetically annotated orthology resource based on 5090 organisms and 2502 viruses. Nucleic Acids Res 47:D309–D314. https://doi.org/10.1093/nar/gky1085.

110. Emms DM, Kelly S. 2015. Orthofinder: solving fundamental biases in whole genome comparisons dramatically improves orthogroup inference accuracy. Genome Biol 16:157. https://doi.org/10.1186/s13059-015-0721-2.

111. Jones P, Binns D, Chang H-Y, Fraser M, Li W, McAnulla C, McWilliam H, Maslen J, Mitchell A, Nuka G, Pesseat S, Quinn AF, Sangrador-Vegas A, Scheremetjew M, Yong S-Y, Lopez R, Hunter S. 2014. Interproscan 5: genome-scale protein function classification. Bioinformatics 30: 1236–1240. https://doi.org/10.1093/bioinformatics/btu031.

112. Dam P, Olman V, Harris K, Su Z, Xu Y. 2007. Operon prediction using both genome-specific and general genomic information. Nucleic Acids Res 35:288–298. https://doi.org/10.1093/nar/gkl1018.

113. Mao X, Ma Q, Zhou C, Chen X, Zhang H, Yang J, Mao F, Lai W, Xu Y. 2014. Door 2.0: presenting operons and their functions through dynamic and integrated views. Nucleic Acids Res 42:D654–D659. https://doi.org/10.1093/nar/gkt1048.

114. Mao F, Dam P, Chou J, Olman V, Xu Y. 2009. Door: a database for prokaryotic operons. Nucleic Acids Res 37:D459–D463. https://doi.org/10.1093/nar/gkn757.